Kinetically Controlled Two-Step Amorphization and Amorphous-Amorphous Transition in Ice

Chuanlong Lin,[1] Xue Yong,[2] John S. Tse,[2,*] Jesse S. Smith,[1] Stanislav V. Sinogeikin,[1] Curtis Kenney-Benson,[1] and Guoyin Shen[1,†]

[1]*HPCAT, Geophysical Laboratory, Carnegie Institution of Washington, Argonne, Illinois 60439, USA*

[2]*Department of Physics and Engineering Physics, University of Saskatchewan, Saskatoon, S7N 5E2 Canada*

(Received 31 March 2017; published 29 September 2017)

We report the results of *in situ* structural characterization of the amorphization of crystalline ice Ih under compression and the relaxation of high-density amorphous (HDA) ice under decompression at temperatures between 96 and 160 K by synchrotron x-ray diffraction. The results show that ice Ih transforms to an intermediate crystalline phase at 100 K prior to complete amorphization, which is supported by molecular dynamics calculations. The phase transition pathways show clear temperature dependence: direct amorphization without an intermediate phase is observed at 133 K, while at 145 K a direct Ih-to-IX transformation is observed; decompression of HDA shows a transition to low-density amorphous ice at 96 K and ~1 Pa, to ice Ic at 135 K and to ice IX at 145 K. These observations show that the amorphization of compressed ice Ih and the recrystallization of decompressed HDA are strongly dependent on temperature and controlled by kinetic barriers. Pressure-induced amorphous ice is an intermediate state in the phase transition from the connected H-bond water network in low pressure ices to the independent and interpenetrating H-bond network of high-pressure ices.

DOI: 10.1103/PhysRevLett.119.135701

The discovery of a pressure-induced transformation from crystalline ice Ih to high-density amorphous (HDA) form at 77 K and 1 GPa in 1984 [1] is a major milestone in the study of the physics and chemistry of ice. Following that, several different amorphous forms have been observed in different temperature and pressure regimes, e.g., low-density amorphous (LDA) ice [1–4], expanded high-density amorphous (eHDA) ice [5], and very high-density amorphous (VHDA) ice [6]. The transformation from LDA to HDA upon compression and structures of LDA and HDA have been well studied using neutron diffraction [7–11]. The first-order-like LDA-to-HDA transition—extrapolated into the no man's land where the temperature is between homogenous nucleation temperature (T_H) of supercooled water and crystallization temperature (T_X) of amorphous ice—was hypothesized to terminate at a second critical point [12,13]. These two phenomena, viz., the pressure-induced amorphization (PIA) of ice Ih and the LDA-HDA transition, were the cornerstones to support the two-liquid model of water [14,15]. In addition, the amorphization of ice Ih and LDA-to-HDA transition have become the prototypical examples in the investigations of solid-state amorphization and amorphous-amorphous transitions of many materials, e.g., α-quartz [16], α-GeO_2 [17], and $AlPO_4$ [18]. Nevertheless, the PIA mechanism and its relation to the two-liquid model of water is still being hotly debated despite extensive efforts devoted to characterizing the amorphization process using volumetric, Raman, neutron and ultrasonic measurements, and theoretical simulations [1,12,19–26]. Fundamental questions still remain regarding the details on the structural evolution and relationship among the structures [15,27,28].

Different mechanisms have been proposed to interpret the amorphization of ice Ih, e.g., thermodynamic melting [1], mechanical instability [19,21], and transient melting [29]. Initially, the PIA was attributed to melting at low temperature [1], implying a thermodynamically driven transition. Later experiments have shown a distinctive change in the transformation mechanism at ~160 K [20]. It was shown that the PIA at low temperatures (<160 K) is a result of mechanical instability in which one of the Born's conditions for solid stability was violated [21]. Furthermore, the PIA could be strongly influenced by deviatoric stress [30], which could result in a precursor crystalline-crystalline transition prior to amorphization [31]. In light of the possible existence of transient melting in solid-solid transition, the PIA of ice Ih was interpreted via a process of virtual melting [29,32]. For ice at low temperature, the behavior of the hexagonal lattice under pressure plays an important role in understanding the nature of amorphization. However, detailed information on pressure-induced structural evolution near the onset of amorphization by *in situ* diffraction methods such as x-ray and neutron diffractions is still lacking. In this Letter, we probed the structural evolution of the hexagonal ice Ih and its corresponding reversible transition (i.e., recrystallization of decompressed HDA) under quasihydrostatic conditions at various temperatures by *in situ* synchrotron x-ray diffraction. As shown below, three important observations were made: (i) the PIA is not a

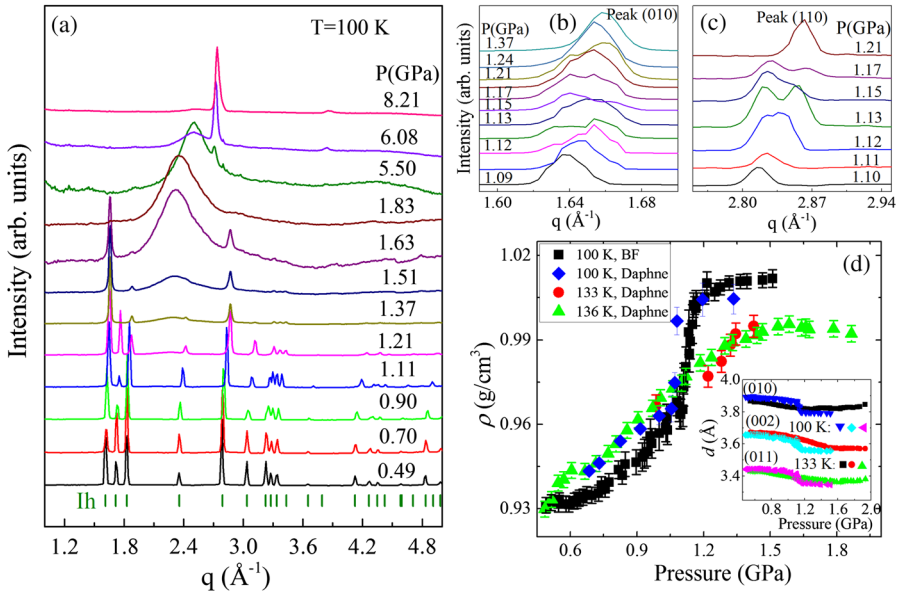

FIG. 1. (a) Structural evolution of compressed ice Ih at 100 K in the quasihydrostatic condition using the back-and-forth approach [34]. The background was subtracted for the typical integrated x-ray diffraction patterns (Fig. S2). At 0.49 GPa, the diffraction pattern is indexed with hexagonal structure of ice Ih (Table S1). (b) and (c)The detailed structural evolutions of (010) and (110) reflections for crystalline ice Ih under compression. (d) Density of the crystalline phases as a function of pressure. The density is calculated using more than six indexed diffraction peaks. BF: back-and-forth approach. The inset in Fig. 1(d) shows pressure-dependent d spacings of three typical diffraction reflections of ice Ih. The slight difference in the initial values of d spacings could be due to the cooling history.

single step process; (ii) at very low pressure (~1 Pa), the HDA can only be recovered at very low temperature, otherwise it transforms to LDA or other crystalline forms of ice; (iii) in the pressure range of this study, there is a crossover in transition mechanism at around 145 K, above which the phase transition of ice is largely thermodynamically controlled and below which it is kinetically controlled.

Distilled deionized water was loaded into the sample chamber in symmetric diamond anvil cells (DAC), together with several ruby spheres (Fig. S1) as pressure marker [33]. To reduce deviatoric stress, the sample was compressed by a "back-and-forth" method or in the environment of pressure medium Daphne 7474 (or 7575) [34]. Loaded DAC were placed in the liquid nitrogen cryostat [47]. Two silicon diode sensors were used to monitor the temperatures with one attached to the holder and the other attached to the gasket in the cell. Double gas membranes on both sides of the DAC were used to control the compression and decompression paths precisely. Angle dispersive x-ray diffraction experiments were performed at beam line 16-ID-B, HPCAT [48], and sector 20-ID-C, Advanced Photon Source, Argonne National Laboratory. Diffraction data were analyzed and integrated using software Fit2D [49]. In integration, background was subtracted (Fig. S2 [34]). Lattice parameters were obtained by fitting diffraction peaks using the Le bail method in the GSAS software [50].

Figure 1(a) shows the diffraction patterns of compressed ice Ih at 100 K under quasihydrostatic conditions using the back-and-forth compression approach (details of the compression method are in the Supplemental Material and Fig. S1 [34]). Crystalline ice Ih with the hexagonal structure is found to co-exist with HDA at 1.21 GPa with the appearance of a halo peak at $Q = 2.25$ Å^{-1}. Above 1.21 GPa, the Bragg reflections of ice Ih gradually lose intensity while the intensity of the halo peak of HDA grows. The amorphization is completed at ~1.8 GPa with the complete disappearance of crystalline peaks. The onset transition pressure and pressure range of amorphization are consistent with previous Raman, volumetric, and ultrasonic measurements [1,22,26]. Upon further compression, the halo peak shifts to higher Q and the amorphous ice finally crystallizes into an ice VIII-like (VIII') phase at ~5.5 GPa [Fig. 1(a)]. The transition pressure is higher than that from a previous report (~4 GPa) [26]. Careful examination of the diffraction patterns from 1.05 to 1.21 GPa reveals splittings of several diffraction peaks [illustrated in Figs. 1(b) and 1(c)]. Above 1.21 GPa, the splittings apparently disappear and the diffraction peaks again can be indexed to the hexagonal structure (Fig. S3). The peak splitting is even more pronounced when ice Ih is compressed at 100 K without the back-and-forth compression technique (Fig. S4), which may be due to the stress effect. Once again, the split diffraction peaks overlap or merge close to the amorphous transition pressure. These observations indicate that there may be a crystalline-crystalline transition preceding amorphization due to shear instability or stress-induced distortions of ice Ih.

The pressure dependence of the d spacings of three main diffraction peaks [(010), (002), and (011)] of ice Ih at 100 K under quasihydrostatic conditions are plotted in the inset

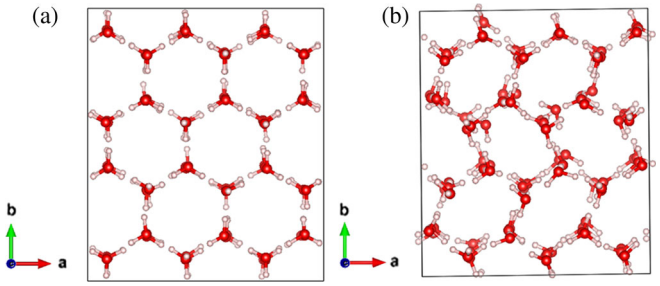

FIG. 2. Theoretical crystal structures of (a) ice Ih and (b) intermediate crystalline phase. The intermediate crystalline phase is a shear-distorted form of ice Ih in the *ab* basal plane due to the softening of C_{66} elastic modulus. The oxygen atom in the intermediate phase have shifted slightly from the original position of ice Ih. Thus, when view down the *c* axis, the oxygen atoms are no longer aligned along the *c* axis as in ice Ih.

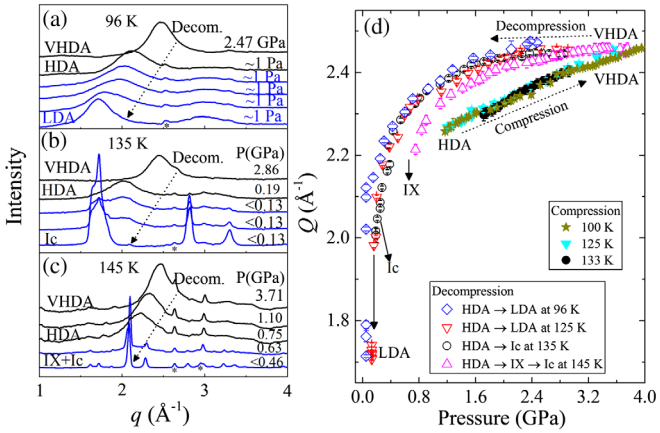

FIG. 3. Structural evolution of amorphous ice under decompression (a) at 96, (b) at 135, and (c) at 145 K. Amorphous ice at 145 K was obtained by heating VHDA from 133 to 145 K. (d) The pressure-dependent Q values of the first sharp peak position of the amorphous ice. The dashed arrows indicate compression and decompression route. The solid arrows indicate the phase transition of HDA under decompression. The peaks marked by stars are from gasket.

of Fig. 1(d) (see more diffraction peaks in Fig. S5). It is found that the *d* spacings decrease gradually with increasing pressure up to 1.05 GPa. Then, an abrupt decrease in the *d* spacings is observed between 1.05 and 1.17 GPa prior to amorphization. Above 1.21 GPa, the variation of the *d* spacings becomes smooth again and the split peaks merge into bands, resulting in a pattern resembling ice Ih. Therefore, the densities can be estimated from unit cell volumes derived from at least six Bragg reflections indexed to ice Ih (Table S1 and S2 [34]) in Fig. 1(d). In agreement with the piston-cylinder measurement, the density is found to increase continuously with pressure below 1.05 GPa [1,22]. At ~1.05–1.2 GPa, the density of crystalline ice increases abruptly corresponding to a densification of ~4%. Above 1.21 GPa, the density increases gradually. This observation demonstrates that at 100 K ice Ih has transformed to a dense crystalline phase *prior* to amorphization under quasi-hydrostatic conditions. In other words, the PIA in ice Ih does not occur in a single step, but is a two-step process. We repeated the back-and-forth compression experiment in run 2 at 100 K and obtained similar results. Ice Ih was also compressed in a pressure medium Daphne 7474 [51,52], and the crystalline-crystalline transition was again reproduced, as shown in Fig. 1(d).

The crystalline-crystalline transformation just prior to the PIA is reproduced by isobaric-isothermal molecular dynamics (MD) calculations using an empirical water TIP4P/ice potential [53] and first-principles density functional method (Fig. S6) [34]. It is found that when the pressure is increased in small incremental steps (0.1 GPa), the calculated density as a function of pressure reveals a structural transition to a dense crystalline phase from ice Ih at 1.2 GPa with the TIP4P/ice potential and at a slightly higher pressure (1.9 GPa) from first-principles MD (Figs. S7 and S8). In both cases, the transformed structure is a shear-distorted form of ice Ih [Figs. 2(a) and 2(b)]. It should be noted that the first-principle density-functional methods even including the crucial van der Waals correction normally still overestimate the transition pressure [54]. In hindsight the theoretical result is not too surprising as it has been shown previously that, from classical MD and neutron inelastic scattering experiments, the C_{66} elastic modulus which is related to the stress-strain relationship in the hexagonal *ab* basal plane, is softened at the pressure just below amorphization. The MD calculations also show that this intermediate phase is only stable within a small pressure region of about 0.2 GPa then it transforms completely into HDA.

To investigate temperature effect on the PIA of ice Ih, ice Ih was compressed under quasihydrostatic conditions at 133, 136, and 145 K. At 133 and 136 K, the *in situ* x-ray diffraction patterns show ice Ih has transformed directly to HDA at 1.2–1.9 GPa (Fig. S9 [34]), followed by a transformation to very high-density amorphous (VHDA) ice at higher pressures [28]. Unlike at 100 K, no abrupt decrease in *d* spacing is observed at 133 and 136 K [inset of Fig. 1(d)] prior to amorphization. Evidently, the gain in thermal energy by raising the temperature by ~33 K is sufficient to trespass the barrier for direct conversion to the amorphous phase. When compressed at 145 K (Fig. S9 [34]), ice undergoes successive crystalline-crystalline transformations: first from Ih to IX at ~0.9 GPa, and followed by a transition to a VIII-like ice at 3.9 GPa. Upon decompression from 5.7 GPa, the VIII-like phase transformed back to ice IX below 0.8 GPa.

We also investigated the decompression of PIA ice at several temperatures. At ~4 GPa, the Q value of the first sharp diffraction peak (FSDP) of the amorphous ice is ~2.46 Å [Fig. 3(d)]. After recovering amorphous ice from ~4 GPa at liquid nitrogen temperature, the Q value of

amorphous ice at ambient pressure is 2.3 $Å^{-1}$, close to the highest value of VHDA reported previously [55]. This indicates that amorphous ice at ~4 GPa is very high-density amorphous ice. Decompression of amorphous ice leads to a continuous transformation from VHDA back to HDA [Figs. 3(a)–3(d)]. Depending on the temperature and pressure, different phase transitions are observed. At 96 K and ~1 Pa (see experimental method in supplementary materials), HDA relaxes to LDA in about 1 h at ~1 Pa with the appearance of a new halo peak at low Q [Fig. 3(a) and Fig. S10]. We also decompressed HDA at 125 K and observed a first-order HDA-to-LDA transition at ~1 Pa (Fig. S10 [34]). At 135 K, HDA transforms to crystalline Ic with stacking fault [Fig. 3(b) and Fig. S10] [56]. We note that the FSDP position of LDA is very close to the first Bragg peak in ice Ic, reflecting their similarities in density and structure as already pointed out in previous reports [2,7]. We note that HDA transforms gradually to LDA at ~1 Pa and ~96 K in hours, with temperature lower than that (~139 K) in the previous report at ~0.02 GPa in piston-cylinder measurement by Winkel *et al.* [57]. This indicates that the relaxation of HDA into LDA depends strongly on pressure.

Upon decompression at 145 K, VHDA obtained by heating the amorphous sample from 133 to 145 K at ~3.7 GPa transforms to HDA and then to ice IX during the decompression process [Fig. 3(c) and Fig. S11]. IX transforms to ice Ic upon further decompression. We also decompress VHDA at 160 K. X-ray diffraction patterns show a transformation from VHDA to VI (Fig. S11 [34]), followed by VI → II → Ic transitions. Comparison of decompressed HDA at different temperatures shows that the relaxation process and phase transitions become slower at low temperatures [Fig. 3(d)], as expected for a thermally activated process. At the pressure close to the transition to the crystalline phase, a sudden drop of the Q value of the amorphous ice was observed [Fig. 3(d)], suggesting a rapid structural relaxation associated with devitrification of HDA.

Figure 4 summarizes the observed phase transitions of compressed ice Ih and decompressed amorphous ice. The HDA and intermediate phases are only observed below 145 K [Fig. 4(a)], which supports the suggestion that HDA is a "frustrated" intermediate state in which at low temperature the system does not possess sufficient thermal energy to overcome the activation barrier required for the reorientation of the hydrogen-bond network to the underlying stable crystalline structure, perhaps ice IV or XII as suggested by previous experiments [58,59]. Incidentally, the Raman spectra of HDA and VHDA [60] are remarkably similar to crystalline ice VI [61,62], implying that HDA is an uncompleted form in the transformation from ice Ih to ice VI. Since there are substantial changes in the H configurations between ice IX and ice VI, i.e., from a three-dimensional (3D) framework to an interpenetrating H-bonding network, the reorientation of the H atoms at

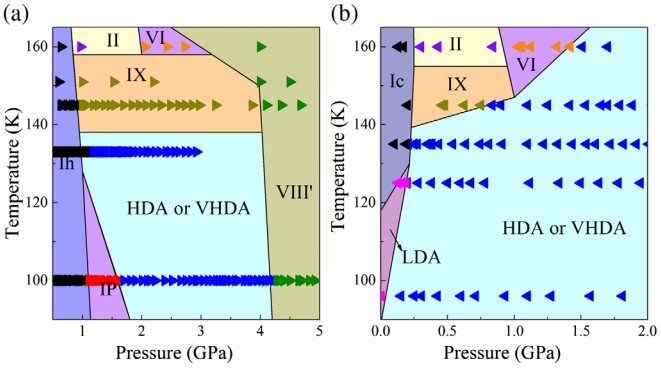

FIG. 4. Summary of phase transitions observed in experiments (a) under slow compression of ice Ih and (b) under slow decompression of amorphous ice. IP stands for the intermediate phase (see texts for more details). HDA or VHDA above 140 K was obtained by heating amorphous samples from 100 or 133 K to corresponding temperatures. The right and left triangle symbols indicate experimental data under compression and decompression, respectively. Crystalline ice Ih and Ic: black, right and left; HDA: blue, right and left; VIII': green, right; IX: olive, right and left; IP: red, right; VI: orange, left; VI: purple, left.

different temperatures will depend on the specific kinetic barriers (activation energies). This view is verified by the comparison of the calculated structure of HDA with the proton ordered form of ice VI, i.e., XV in Fig. S12 [34]. There is a crossover at around 145 K. Above 145 K, the thermal energy is sufficient to bypass the amorphous state and lead to successive crystalline-to-crystalline transitions [Fig. 4(a)], which are thermodynamically driven pathways without the metastable amorphous structure.

For the decompression of amorphous ice, HDA transforms to LDA with local structure similar to ice Ih at lower temperatures [7]. It should be noted that previous research has shown that HDA can exist at 96 K and 1 atm [63]. Here, our x-ray diffraction shows gradual relaxation of HDA into LDA at ~1 Pa and 96 K. Therefore, it is not unreasonable to speculate that LDA will eventually transform to crystalline ice Ic at lower pressure. The LDA is a "kinetically arrested" intermediate amorphous state in the large hysteresis loop of the relaxation process of HDA back to crystalline ice I [64,65]. Comparison of the Raman spectra [60] shows that VHDA has a local structure similar to ice VI. Analysis of the MD calculation shows the formation of independent H-bond network in the structure of HDA and VHDA (Fig. S12). Thus, we may anticipate that the decompression of VHDA will lead to the thermodynamically controlled phase transitions of VHDA → VI → II → Ic if the thermal energy is sufficient, as found in our x-ray measurement at 160 K [Fig. 4(b) and Fig. S11], whereas kinetically controlled VHDA → HDA → LDA transitions will be observed at low temperature due to insufficient thermal energy required for the rearrangement of the H-bonded network. The comparison of the phase transitions in compressed Ih and decompressed HDA suggests

that the PIA is a reversible but kinetically controlled process. Depending on the temperature, intermediate phases may occur in the compression-induced amorphization of ice Ih or decompression-induced crystallization of HDA.

We thank Dr. S. Desgreniers and Dr. K. Murata for the Daphne 7474 and 7575 oil and F. Zou for technical support. This research was supported by DOE-BES, Division of Materials Sciences and Engineering under Award No. DE-FG02-99ER45775. HPCAT operation is supported by DOE-NNSA under Award No. DE-NA0001974, with partial instrumentation funding by NSF. Sector 20 facilities at the Advanced Photon Source, and research at these facilities, are supported by the U.S. Department of Energy—Basic Energy Sciences, the Canadian Light Source and its funding partners, and the Advanced Photon Source. The Advanced Photon Source is a U.S. Department of Energy (DOE) Office of Science User Facility operated for the DOE Office of Science by Argonne National Laboratory under Contract No. DE-AC02-06CH11357. X. Y. acknowledges financial support from China Scholarship Council.

*Corresponding author.
john.tse@usask.ca
†Corresponding author.
gshen@ciw.edu

[1] O. Mishima, L. D. Calvert, and E. Whalley, Nature (London) **310**, 393 (1984).
[2] O. Mishima, L. D. Calvert, and E. Whalley, Nature (London) **314**, 76 (1985).
[3] K. Winkel, D. T. Bowron, T. Loerting, E. Mayer, and J. L. Finney, J. Chem. Phys. **130**, 204502 (2009).
[4] J. J. Shephard, S. Klotz, M. Vickers, and C. G. Salzmann, J. Chem. Phys. **144**, 204502 (2016).
[5] R. J. Nelmes, J. S. Loveday, T. Strassle, C. L. Bull, M. Guthrie, G. Hamel, and S. Klotz, Nat. Phys. **2**, 414 (2006).
[6] T. Loerting, C. Salzmann, I. Kohl, E. Mayer, and A. Hallbrucker, Phys. Chem. Chem. Phys. **3**, 5355 (2001).
[7] J. L. Finney, A. Hallbrucker, I. Kohl, A. K. Soper, and D. T. Bowron, Phys. Rev. Lett. **88**, 225503 (2002).
[8] S. Klotz, G. Hamel, J. S. Loveday, R. J. Nelmes, M. Guthrie, and A. K. Soper, Phys. Rev. Lett. **89**, 285502 (2002).
[9] J. L. Finney, D. T. Bowron, A. K. Soper, T. Loerting, E. Mayer, and A. Hallbrucker, Phys. Rev. Lett. **89**, 205503 (2002).
[10] S. Klotz, T. Strassle, G. Hamel, R. J. Nelmes, J. S. Loveday, G. Rousse, B. Canny, J. C. Chervin, and A. M. Saitta, Phys. Rev. Lett. **94**, 025506 (2005).
[11] S. Klotz, T. Strassle, A. M. Saitta, G. Rousse, G. Hamel, R. J. Nelmes, J. S. Loveday, and M. Guthrie, J. Phys. Condens. Matter **17**, S967 (2005).
[12] O. Mishima and H. E. Stanley, Nature (London) **396**, 329 (1998).
[13] P. H. Poole, F. Sciortino, U. Essmann, and H. E. Stanley, Nature (London) **360**, 324 (1992).
[14] K. Amann-Winkel, R. Bohmer, F. Fujara, C. Gainaru, B. Geil, and T. Loerting, Rev. Mod. Phys. **88**, 011002 (2016).
[15] P. Gallo, K. Amann-Winkel, C. A. Angell, M. A. Anisimov, F. Caupin, C. Chakravarty, E. Lascaris, T. Loerting, A. Z. Panagiotopoulos, J. Russo, J. A. Sellberg, H. E. Stanley, H. Tanaka, C. Vega, L. Xu, and L. G. M. Pettersson, Chem. Rev. **116**, 7463 (2016).
[16] R. J. Hemley, A. P. Jephcoat, H. K. Mao, L. C. Ming, and M. H. Manghnani, Nature (London) **334**, 52 (1988).
[17] J. P. Itie, A. Polian, G. Calas, J. Petiau, A. Fontaine, and H. Tolentino, Phys. Rev. Lett. **63**, 398 (1989).
[18] M. B. Kruger and R. Jeanloz, Science **249**, 647 (1990).
[19] J. S. Tse, J. Chem. Phys. **96**, 5482 (1992).
[20] O. Mishima, Nature (London) **384**, 546 (1996).
[21] J. S. Tse, D. D. Klug, C. A. Tulk, I. Swainson, E. C. Svensson, C. K. Loong, V. Shpakov, V. R. Belosludov, R. V. Belosludov, and Y. Kawazoe, Nature (London) **400**, 647 (1999).
[22] E. L. Gromnitskaya, O. V. Stal'gorova, V. V. Brazhkin, and A. G. Lyapin, Phys. Rev. B **64**, 094205 (2001).
[23] T. Strassle, A. M. Saitta, S. Klotz, and M. Braden, Phys. Rev. Lett. **93**, 225901 (2004).
[24] T. Strassle, S. Klotz, G. Hamel, M. M. Koza, and H. Schober, Phys. Rev. Lett. **99**, 175501 (2007).
[25] T. Strassle, A. Caviezel, B. Padmanabhan, V. Y. Pomjakushin, and S. Klotz, Phys. Rev. B **82**, 094103 (2010).
[26] R. J. Hemley, L. C. Chen, and H. K. Mao, Nature (London) **338**, 638 (1989).
[27] C. A. Tulk, C. J. Benmore, J. Urquidi, D. D. Klug, J. Neuefeind, B. Tomberli, and P. A. Egelstaff, Science **297**, 1320 (2002).
[28] T. Loerting, W. Schustereder, K. Winkel, C. G. Salzmann, I. Kohl, and E. Mayer, Phys. Rev. Lett. **96**, 025702 (2006).
[29] V. I. Levitas, Phys. Rev. Lett. **95**, 075701 (2005).
[30] J. Haines, J. M. Leger, F. Gorelli, and M. Hanfland, Phys. Rev. Lett. **87**, 155503 (2001).
[31] K. J. Kingma, R. J. Hemley, H. K. Mao, and D. R. Veblen, Phys. Rev. Lett. **70**, 3927 (1993).
[32] V. I. Levitas, B. F. Henson, L. B. Smilowitz, and B. W. Asay, Phys. Rev. Lett. **92**, 235702 (2004).
[33] H. K. Mao, J. Xu, and P. M. Bell, J. Geophys. Res. **91**, 4673 (1986).
[34] See Supplemental Material at http://link.aps.org/supplemental/10.1103/PhysRevLett.119.135701 for experimental details and molecular dynamics simulation, which includes Refs. [35–46].
[35] R. Hrubiak, S. Sinogeikin, E. Rod, and G. Y. Shen, Rev. Sci. Instrum. **86**, 072202 (2015).
[36] J. A. Hayward and J. R. Reimers, J. Chem. Phys. **106**, 1518 (1997).
[37] U. Essmann, L. Perera, M. L. Berkowitz, T. Darden, H. Lee, and L. G. Pedersen, J. Chem. Phys. **103**, 8577 (1995).
[38] W. Smith, C. W. Yong, and P. M. Rodger, Mol. Simul. **28**, 385 (2002).
[39] S. Grimme, J. Comput. Chem. **27**, 1787 (2006).
[40] S. Grimme, J. Antony, S. Ehrlich, and H. Krieg, J. Chem. Phys. **132**, 154104 (2010).
[41] S. Grimme, S. Ehrlich, and L. Goerigk, J. Comput. Chem. **32**, 1456 (2011).
[42] M. Dion, H. Rydberg, E. Schroder, D. C. Langreth, and B. I. Lundqvist, Phys. Rev. Lett. **92**, 246401 (2004).

[43] J. Klimes, D. R. Bowler, and A. Michaelides, Phys. Rev. B **83**, 195131 (2011).
[44] K. Rottger, A. Endriss, J. Ihringer, S. Doyle, and W. F. Kuhs, Acta Crystallogr. Sect. B **50**, 644 (1994).
[45] C. G. Salzmann, P. G. Radaelli, E. Mayer, and J. L. Finney, Phys. Rev. Lett. **103**, 105701 (2009).
[46] J. Russo and H. Tanaka, Nat. Commun. **5**, 3556 (2014).
[47] S. V. Sinogeikin, J. S. Smith, E. Rod, C. L. Lin, C. Kenney-Benson, and G. Y. Shen, Rev. Sci. Instrum. **86**, 072209 (2015).
[48] J. S. Smith, S. V. Sinogeikin, C. L. Lin, E. Rod, L. G. Bai, and G. Y. Shen, Rev. Sci. Instrum. **86**, 072208 (2015).
[49] A. P. Hammersley, S. O. Svensson, M. Hanfland, A. N. Fitch, and D. Hausermann, High Press. Res. **14**, 235 (1996).
[50] B. H. Toby, J. Appl. Crystallogr. **34**, 210 (2001).
[51] S. Sasaki, S. Kato, T. Kume, H. Shimizu, T. Okada, S. Aoyama, F. Kusuyama, and K. Murata, Jpn. J. Appl. Phys. **49**, 106702 (2010).
[52] K. Murata, K. Yokogawa, H. Yoshino, S. Klotz, P. Munsch, A. Irizawa, M. Nishiyama, K. Iizuka, T. Nanba, T. Okada, Y. Shiraga, and S. Aoyama, Rev. Sci. Instrum. **79**, 085101 (2008).
[53] J. L. F. Abascal, E. Sanz, R. G. Fernandez, and C. Vega, J. Chem. Phys. **122**, 234511 (2005).
[54] B. Santra, J. Klimes, D. Alfe, A. Tkatchenko, B. Slater, A. Michaelides, R. Car, and M. Scheffler, Phys. Rev. Lett. **107**, 185701 (2011).
[55] C. G. Salzmann, T. Loerting, S. Klotz, P. W. Mirwald, A. Hallbrucker, and E. Mayer, Phys. Chem. Chem. Phys. **8**, 386 (2006).
[56] T. C. Hansen, M. M. Koza, and W. F. Kuhs, J. Phys. Condens. Matter **20**, 285104 (2008).
[57] K. Winkel, M. Bauer, E. Mayer, M. Seidl, M. S. Elsaesser, and T. Loerting, J. Phys. Condens. Matter **20**, 494212 (2008).
[58] S. Klotz, G. Hamel, J. S. Loveday, R. J. Nelmes, and M. Guthrie, Z. Kristallogr. **218**, 117 (2003).
[59] J. S. Tse, D. D. Klug, M. Guthrie, C. A. Tulk, C. J. Benmore, and J. Urquidi, Phys. Rev. B **71**, 214107 (2005).
[60] T. Loerting, C. Salzmann, I. Kohl, E. Mayer, and A. Hallbrucker, Phys. Chem. Chem. Phys. **3**, 5355 (2001).
[61] J. P. Marckmann and E. Whalley, J. Chem. Phys. **41**, 1450 (1964).
[62] T. F. Whale, S. J. Clark, J. L. Finney, and C. G. Salzmann, J. Raman Spectrosc. **44**, 290 (2013).
[63] C. A. Tulk, C. J. Benmore, J. Urquidi, D. D. Klug, J. Neuefeind, B. Tomberli, and P. A. Egelstaff, Science **297**, 1320 (2002).
[64] J. S. Tse and D. D. Klug, Phys. Chem. Chem. Phys. **14**, 8255 (2012).
[65] N. J. English and J. S. Tse, Chem. Phys. Lett. **609**, 54 (2014).